Meccanica
DOI 10.1007/s11012-017-0762-6

Robotically controlled scale-model testing of masonry vault collapse

Cristián Calvo Barentin · Tom Van Mele · Philippe Block

Received: 21 December 2016 / Accepted: 11 September 2017

Abstract Scale-model testing can be used to understand the equilibrium and validate the computational modelling of discrete-element assemblies subjected to external loads or support displacements. This paper proposes a novel approach to investigate the collapse of discrete-element assemblies using 3D-printed scale models manipulated with force-sensitive robotic arms combined with an optical measuring system. To demonstrate that this provides a more flexible and comprehensive solution for the assessment of the structural behaviour of unreinforced masonry structures, the same setup is used to conduct different types of experiments on a 3D-printed model of a cross vault. First, the robotic arms are used to apply a point load in different locations while measuring the resistance of the vault until collapse. In a second experiment, the robotic arms are used to simulate the effect of progressive differential settlement of the supports of the vault. The trajectory along which the displacement of the support is applied is based on real-time measurements by the force-sensitive robots of the occurring outward thrust.

Keywords Masonry · Vaults · Collapse · Scale-model testing · Stability · Lightweight robots · Force sensing · As-built geometry

C. Calvo Barentin · T. Van Mele · P. Block (✉)
ETH Zurich, Institute of Technology in Architecture, Stefano-Franscini-Platz 1, Zurich, Switzerland
e-mail: block@arch.ethz.ch

1 Introduction

Based on the principle that the stability of unreinforced masonry structures depends primarily on their geometry rather than the strength of their individual components [9], scale-model testing is an essential tool to develop understanding of the complex three-dimensional collapse behaviour of vaulted masonry structures and discrete-element assemblies in general. With the emergence of computational methods for the analysis of structural behaviour, the use of scale-model testing has been limited to specific problems such as the stability of masonry structures [1]. For many of these problems, computational methods are still under active development, and scale-model tests are necessary to validate the computational results. Usually, testing setups are mechanically complex and designed for specific tasks. To perform different tests, complicated and expensive modifications or even entirely different setups are typically needed. This paper presents a novel approach to the physical scale modelling of the collapse of masonry assemblies, based on 3D printing and using force-sensitive robotic arms as testing devices (Fig. 1) combined with an optical measuring system.

The robots can be programmed to apply any force with a controlled position, direction, sense, and magnitude, without having to change the specific testing setup. This allows for flexible manipulation and deformation of models, while measuring forces at

Published online: 05 October 2017

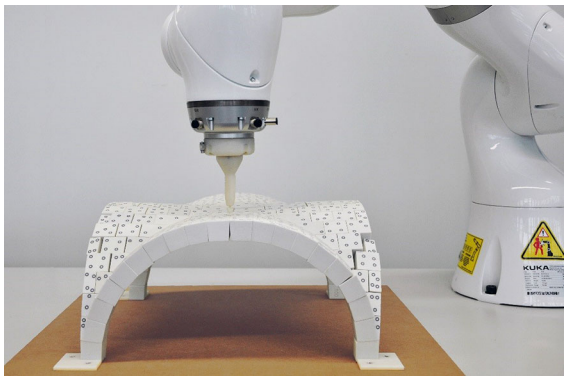

Fig. 1 Force-sensitive robotic arm applying a vertical point load on the scale model of a cross vault

the end effectors of the robots in real-time. With the optical measuring system the imperfections of the as-built scale model compared to the perfect digital model can be assessed, and displacement of all individual blocks during the tests tracked. This detailed geometric and structural data, collected by the different components of the proposed setup, can be used as a base for qualitative and quantitative studies of the collapse behaviour of different vault geometries subjected to varying boundary conditions. It can furthermore be used to calibrate computational simulations, e.g. based on the discrete-element modeling method, with real data such that reliable parametric studies of the collapse mechanisms of different masonry structures can be performed. This paper is mainly focused on demonstrating the potential and flexibility of the robotic system in performing tests on scale models. The paper shows two different test cases with the intent of demonstrating some of the added capabilities of the technique compared to commonly adopted experimental methods. An interesting possibility is the management of data in real time, allowing to take into account external forces/displacements on the model to modify the behaviour of the robotic arms during the test. The outline of the paper is as follows. Section 2 discusses the importance of the use of scale-model testing for the understanding of the structural behaviour of complex structures. In Sect. 3, the possibilities of using force-sensitive robotic arms for scale-model testing of vaulted masonry structures is discussed. The testing procedure with the proposed setup and the acquisition and processing of measurement data are described in Sect. 4. Two example tests are described in Sect. 5, while Sect. 6 provides conclusions and an outlook to future work.

2 Scale-model testing

The use of scale models has always been important in engineering for two reasons: the data collected during the testing process can be used to define a mathematical model of the analysed structural form; and, the results can be used to validate the mathematical model by comparing the predictions from the model and the results from the tests. Furthermore, scale-model testing has been important to increase the confidence of designers on the structural stability of their designs and how they would respond to different expected load scenarios [1]. Medieval builders based their designs on sequences of geometric operations, which were developed and validated over generations (Fig. 2). Although they never had a scientific understanding of why these structures were able to stand, empirical observations led them to develop a deep understanding on how this type of structures behave. These observations allowed them to identify successful reoccurring geometrical patterns that became the base of the Gothic theory of structural design [10]. In those times, builders relied on the fact that, for masonry structures, stability is independent of scale, to linearly scale their design. Even though assumed, there is no direct evidence that medieval builders actually used scale models to analyse designs of masonry structures. The first recorded traces of scale-model testing date back to the experiments of Danyzy [6], who used plaster models to investigate the collapse mechanisms of masonry arches and buttresses (Fig. 3).

Previous research on combined numerical and physical modelling of discrete-element assemblies collapse has mainly focused on support displacement. In Theodossopoulos et al. [18], a dead-weight load test is performed on a scale model of the vault of Abbey Church of Holyrood in Edinburgh. Subsequently, a support displacement test is also performed. The obtained data is compared with Finite Element Modelling (Fig. 4). In Quiñonez et al. [13], two 3D-printed domes are tested to collapse due to uniform support displacements. The obtained experimental data is compared with analytical predictions. In Van Mele et al. [19], three different support displacement tests (diagonal, transverse, and vertical) are performed

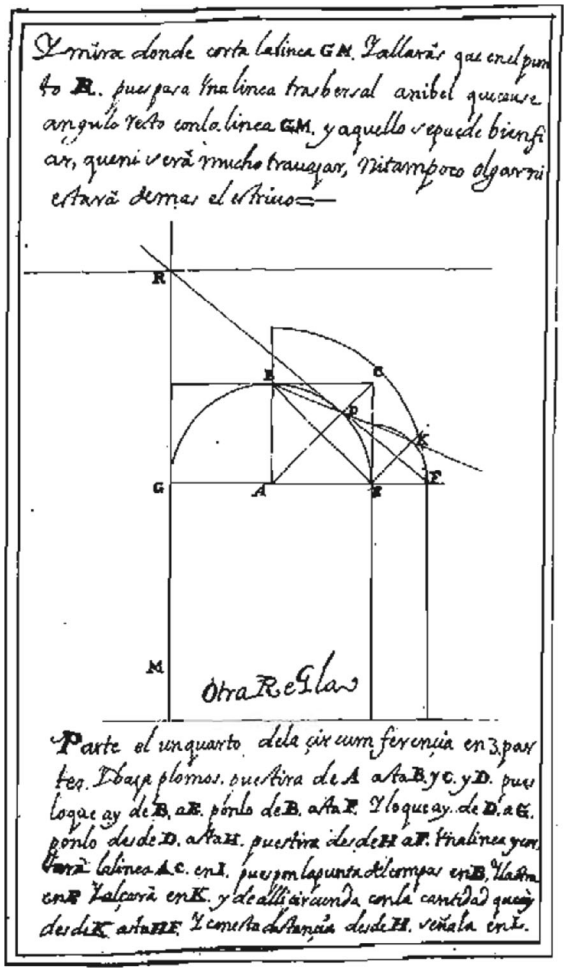

Fig. 2 Geometric rules used by Rodrigo Gil to obtain a stable geometry for an abutment pier [7, 10]

on a masonry groin vault. The obtained experimental data is compared with Discrete Element Modelling results. Figure 5 shows the testing setup used by Rossi et al. [15] to analyse the seismic, in-plane displacement capacity of masonry cross vaults. In Rossi et al. [16], the collapse mechanisms and the ultimate displacement capacity of a 3D-printed pavilion vault on spreading supports are analysed. In all cases, deviations in the geometry of the printed blocks, and positioning tolerances accumulated during the assembly process were not taken into account in the computational model, which makes a quantitative comparison of results difficult.

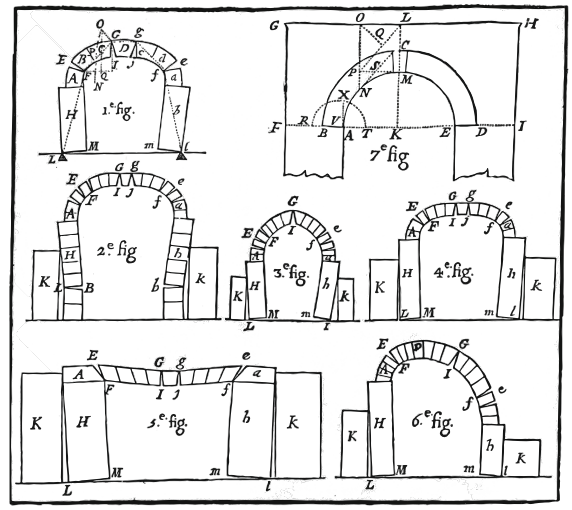

Fig. 3 Masonry arch collapse mechanisms study [6]

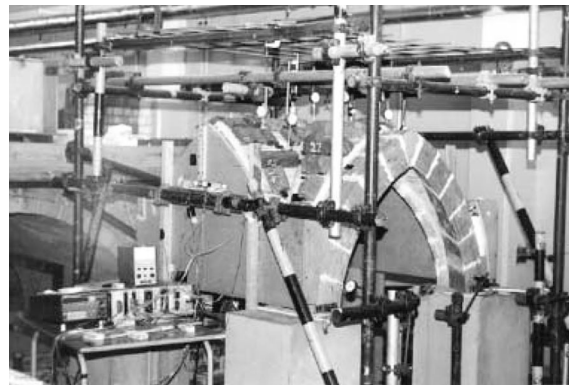

Fig. 4 Testing setup used to assess the response of a scale-model vault to service loads [18]

3 Scale-model testing using force-sensitive robotic arms

Research on the use of industrial robots in the fields of architecture and construction is mostly related to the execution of predefined tasks in automated fabrication or assembly processes. Traditionally, these robots move blindly, just following instructions, without taking into account external inputs, and without verifying if the task is being performed correctly. The arrival of a new generation of robotic arms, capable of sensing external forces acting on their end-effectors, or in any part of their bodies [2, 5], opens up new perspectives for the use of robotic arms; for example, for the analysis of the structural behaviour of (small-scale) physical models. Lightweight force-

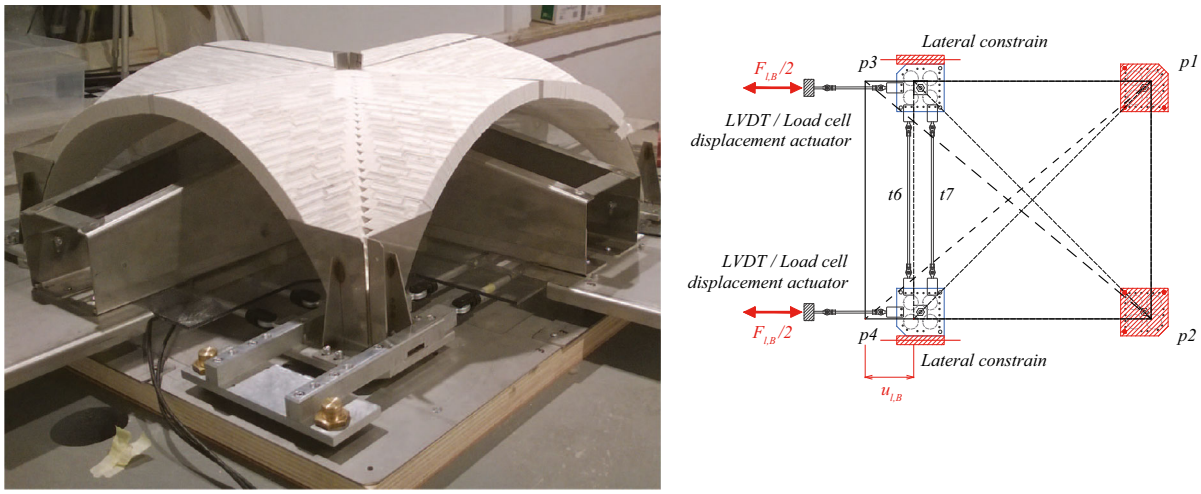

Fig. 5 Testing setup for the assessment of the behaviour of a cross vault subjected to differential support displacements [15]

sensitive robots were developed for different applications than the ones of classical industrial robots. Unlike the latter, where the emphasis is on high absolute positioning accuracy, lightweight robots are designed for interaction with humans in uncontrolled environments. For this reason, the design of these robotic arms is focused on the ability to sense the torques at each joint. This feature allows lightweight robots to avoid collisions in an unknown environment through sensing. Their complete state or pose is defined not just by position and velocity, as it is in the case for industrial robots, but also by joint torques and their derivatives [2, 5]. As a result, researchers are now able to program adaptive behaviour not only in response to changing external conditions and measured geometry, but also considering force data provided by the robots themselves. Because of these capabilities, the use of force-sensitive robotic arms opens up new possibilities for the physical simulation and measurement of the collapse behaviour of vaulted masonry structures. For example, different types of tests can be performed on the same model, simply by changing the pose of the robots rather than modifying the entire testing setup. This is because, with six and seven degrees of freedom, robotic arms are designed to reach any point inside of its dexterous workspace with any given end-effector orientation. In addition, the force readings of the robotic arms can be used as parameters to define, in real-time, the location and orientation of the end effector. By constraining the way how these robotic arms react to external forces, it is possible to define interactions between scale model and testing setup. Reaction forces measured on the end effectors of the robotic arms can be used to modify the way they act on the scale model.

4 Methodology

In this section, we describe the different steps involved in a testing procedure with the proposed setup, using a model of a masonry cross vault as an example.

4.1 Computational model

A digital model of the vault was constructed in the 3D CAD software Rhinoceros [14], and used as a basis for the physical and computational model. The cross-vault geometry was generated from the intersection of two semi-circular barrel vaults with an inner and outer radius of 150 and 175 mm respectively. The vault is discretised in blocks (two types for the webs and ten types for the groins) whose geometrical characteristics and pattern do not reproduce those of typical masonry cross vault. The purpose of the paper, indeed, is not to focus specifically on the understanding of collapse mechanisms of masonry vaults, but to demonstrate how, with the use of this innovative robotic setup, it is possible to model complex structural behaviours, which common testing setups cannot fulfil.

4.2 Physical collapse simulation

The scale-model tests were conducted in the testing laboratory developed by the Block Research Group (BRG) at ETH Zurich. The testing setup consists of two main components: a robotic setup, composed of two force-sensitive robotic arms, and a high-precision optical measuring system (Fig. 6).

4.2.1 3D-printed scale model

The individual blocks of the scale model were printed with a Stratasys Connex3 Objet500 3D printer [17], which is based on polyjet 3D-printing technology. Each block of the vault was labelled with a unique four-dot pattern used as markers to trace its rigid-body position, orientation, and displacement (Fig. 7). The accuracy of the printer is 0.1 mm, which is sufficient to print a model with the necessary precision. The individual blocks of the scale model were printed using VeroWhitePlus, a opaque rigid photopolymer. Using ten random block samples, the average density of the material was determined to be $1.412 \pm 0.06\,\mathrm{g/cm^3}$ and the friction angle $38^\circ \pm 4^\circ$.

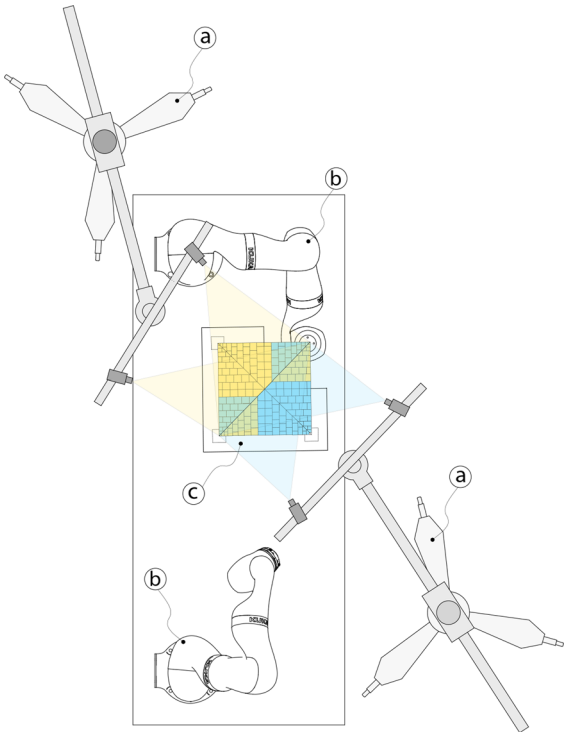

Fig. 6 Masonry scale-model testing in the BRG lab at ETH Zurich: **a** optical measuring system, **b** force-sensitive robotic arms, and **c** 3D-printed scale model

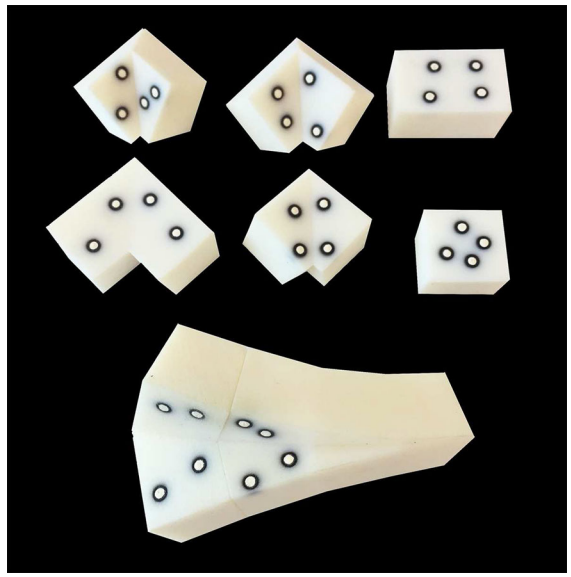

Fig. 7 3D-printed pieces with the tracking/vision markers using unique four-dot pattern

4.2.2 Robot-controlled boundary conditions

The robotic setup used for the scale-model tests consists of two lightweight, force-sensitive robotic arms, model KUKA LBR iiwa 14 R820, with a payload of 14 kg, and maximum range of 820 mm [11]. With seven joints, which means seven degrees of freedom, the kinematic system of these force-sensitive robotic arms is redundant. This implies that any location and orientation in the work envelope of the robotic arm can be accomplished by using more than one joint configuration. Note that these force-sensitive robotic arms use a controller kernel that enables the object-oriented programming of complex robotic behaviours using torque sensors and I/O data. Two custom-designed end effectors were 3D printed with the above-mentioned printer. The design of these end effectors responds to specific requirements of each type of scale-model test (Fig. 8).

4.2.3 Optical measuring system

The PONTOS dynamic 3D motion analysis system by GOM [8] was used as an optical measuring system to scan the exact position and orientation of each block of

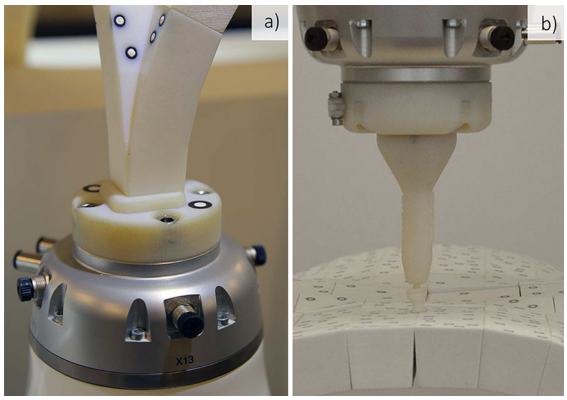

Fig. 8 Custom robot end effectors, **a** for the support displacement tests, and **b** for the point load tests

the cross vault using the four-dot patterns (Fig. 6). Figure 9 shows an example of the results obtained from the PONTOS system. The arrows show the magnitude of the displacement in *X*, *Y*, and *Z* directions. Using triangulation, PONTOS computes the coordinates of each marker from two images. The marker should be visible in both images to determine its position. Because of the high curvature of the model, two sensors were used to track all markers on the extrados of the model. The two obtained point clouds were combined using fixed reference markers placed on the base of the model. After this, the coordinates and absolute deviations of each point in the cloud were converted into data tables. The version of the software used to track the markers during the test was PONTOS v6.3.0-5. The stereo camera system used was equipped with two Baumer TXG50i cameras with Schneider Kreuznach CINEGON 1.4/12 lenses, set at a frame rate of 1 frame per second, a focal ratio of 5.6, and a shutter speed of 7 ms. Each system was equipped with two high-power LED lamps. The accuracy of the measurements depends on the calibration of each system. Usually, the deviation of the sensor is between 0.01 and 0.05 pixels, which means that depending on the distance from the marker to the camera the accuracy of the measurement will change. In the calibration used for the presented tests, the average deviation of both systems was 0.025 pixels.

4.3 Data model

By using an automated testing setup it is possible to have a fluent communication between physical and computational model. The data obtained from the scale model can be transferred to the computational model, to address characteristics that otherwise are too complex to include as parameters in the computational model. The advantage of this is that the computational model turns into a more realistic model, and not just a simplified abstraction of the physical model. In addition, it is possible to assess parameters like the imperfections of the 3D-printed model or the inaccuracy of the assembly process.

4.3.1 As-built geometry

The point cloud obtained from the PONTOS system, and the point cloud obtained from the digital model (reference point cloud), are used to map the deviations of all individual blocks of the scale model. First, an Iterative Closest Point (ICP) algorithm is used to minimise the difference between the two point clouds. This alghoritm, first introduced by Besl and McKay [4], iteratively finds the transformation between the scanned point cloud and the reference point cloud by minimising the distance and rotation between them.

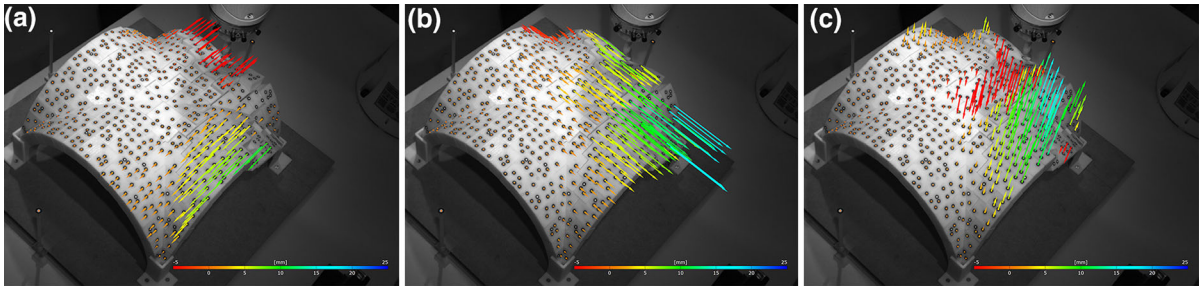

Fig. 9 Deformations along the **a** *X*, **b** *Y*, and **c** *Z* axes of a 3D-printed scale model of a cross vault due to a vertical point load. The arrows show the direction and magnitude of the displacements. The colour gradients show the range of displacement going from 5 mm (red) to 25 mm (blue). (Colour figure online)

Second, the four-point pattern of all individual blocks of the reference point cloud are mapped, together with their corresponding block geometry, in a data structure. Third, for each of these groups, a Nearest Neighbor Search is used to map the four nearest points in the source point cloud [3]. Finally, for each block, a transformation matrix is calculated using the related four-dot patterns in both point clouds. These transformation matrices are used to modify the location and orientation of each block in the digital model (Fig. 10).

4.4 Computational analysis

The detailed force and displacement data collected by the different components of the proposed setup can then be used for further analysis of the collapse behaviour of the vault. For example, the data can serve to calibrate a discrete-element model for a detailed analysis of every stage of the simulated collapse behaviour [19]. However, this kind of computational simulations will not be discussed in this paper.

5 Example tests

The deformation of the cross-vault model is measured and observed in three different cases. In the first case, a force-sensitive robotic arm applies vertical point loads to various locations of the extrados of the vault. In the second case, the robotic arm is used to simulate settlement of one of the supports of the vault in the direction of the occurring measured thrust. In the third case, two robotic arms impose differential settlements onto two neighbouring supports and then simulate consolidation of the supporting soil.

5.1 Point loads

For the point load tests, one of the robotic arms was used to push vertically on the extrados of the vault with a constant velocity of 2 mm/s, while measuring the resistance of the vault against this imposed displacement. Six tests were performed by applying force at different locations on the extrados of one of the webs, between the centre and the edge of the vault, as depicted in Fig. 11. Figure 12 plots the imposed displacement versus the measured resistance of the vault for each of the tests. In the first test, the load is applied to the intersection point of the four blocks forming the crown. Its force/displacement graph is the black curve in Fig. 12. Relevant stages of the observed response behaviour are depicted in Fig. 13. At first, the resistance of the vault increases proportionately with the displacement until a maximum force is measured after approximately 13 s, at a displacement of 26 mm. Note that this increase of resistance, i.e. that the point load increases, just before collapse can be attributed to the vault becoming more shallow (due to hinging) until a mechanism forms, with collapse as result. This shallower arch has more maximum horizontal thrust capacity and thus needs a higher vertical force to push the thrust line out of the section [12]. During this process, the vault forms a continuous crack around the entire vault, across the webs, creating a hinge that separates the central part from the boundary arches (Fig. 13). After approximately 14 s, at a displacement of 28 mm, one of the crown blocks starts to slip out of the assembly, creating space for the other blocks to settle, which results in a sudden drop of the resisting force to 9 N. From then on, the robot pushes the block further out of the assembly while the measured resistance gradually decreases, until it falls to the ground at a displacement of 40 mm when the resistance reduces to zero. During the second test, both the

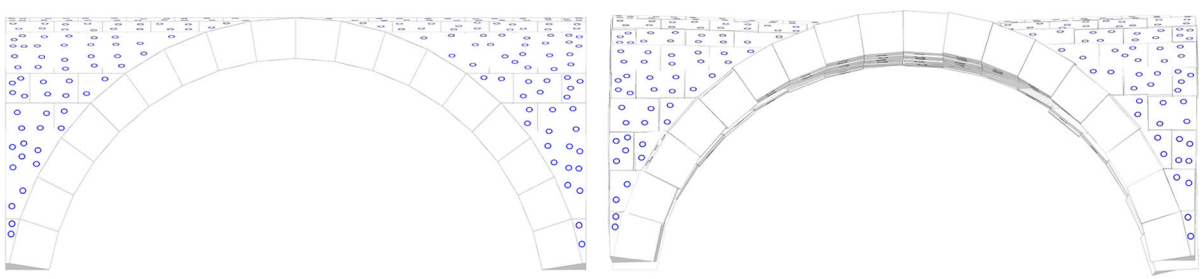

Fig. 10 Digital model, before and after using the ICP algorithm

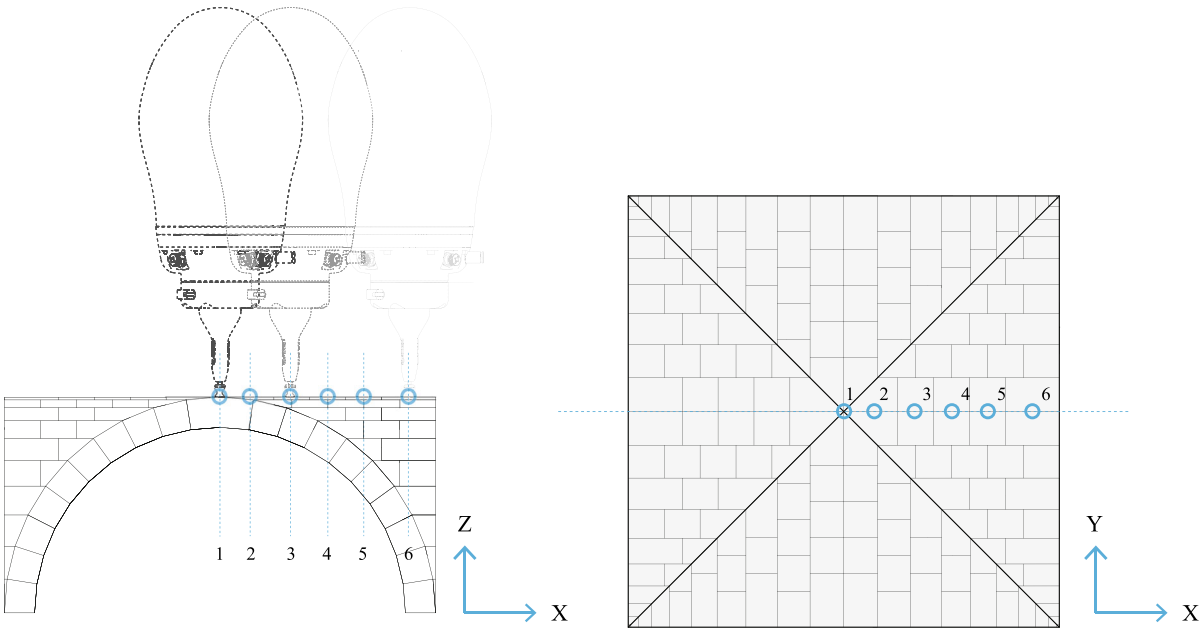

Fig. 11 Point loads: six different vertical point-load cases applied along a line from the crown to the edge of one of the webs of the cross-vault model

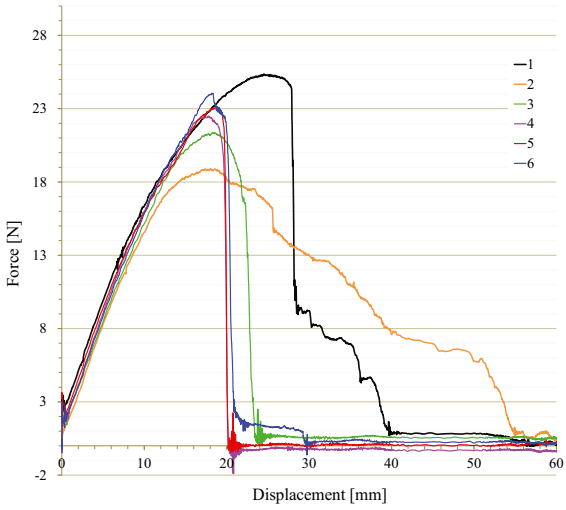

Fig. 12 Point loads: force versus displacement graph of the point load tests. Three types of response curves can be distinguished

measured and observed behaviour are different. In this case, the load is applied slightly off-centre, on only two of the keystone blocks. The force/displacement progression of this test is represented by the orange curve in Fig. 12, and relevant stages of the observed behaviour are depicted in Fig. 14. Initially, measured force and imposed displacement increase proportionately as before. However, in this case, after approximately 10 s (and thus 20 mm of displacement) the two keystone blocks simply start to slide out. As a result, the resistance of the vault decreases gradually until the blocks fall out of the assembly, at just over 35 mm of displacement when the resistance decreases to zero. The cracks that allow the vault to change geometry and absorb the imposed deformation now only developed on one side of the structure. Again, as soon as the keystone blocks fell out, the vault re-settled in a more compact state. A third type of response behaviour was observed in all other tests. There, the web always behaved independently from the rest of the vault, forming a four-hinge mechanism that eventually caused a local collapse of the web, but not of the entire vault. This can be seen in Fig. 15, which depicts relevant stages of test 5. Note that this behaviour of the web is similar to that of an arch under the same loading conditions. As soon as the the partial collapse occurs, the resistance of the vault drops to zero in all tests (Fig. 12). In general, the displacement and resistance thus initially increase proportionately [12]. Then, either one or more of the loaded blocks start to slide and eventually fall out, or the vault develops a mechanism that leads to (partial) collapse. In case of the former, we can observe a gradual

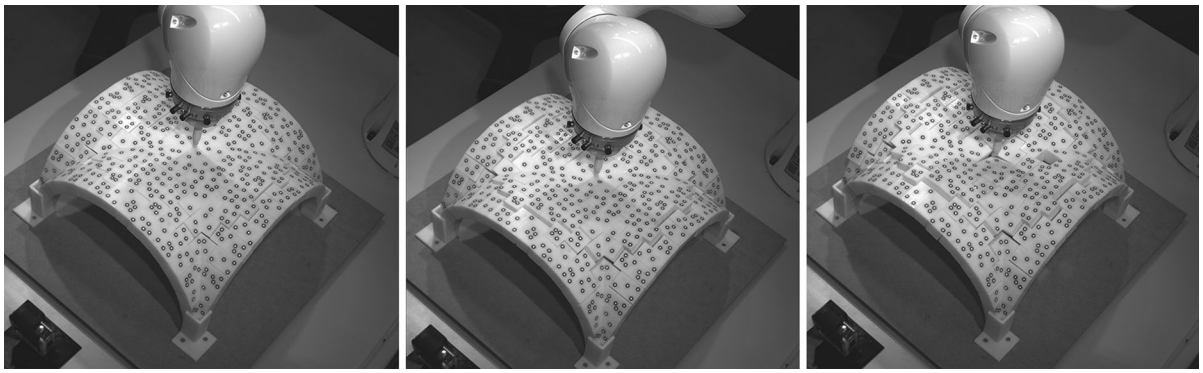

Fig. 13 Point loads: significant stages of load test 1. The point load is applied to the intersection point of the four keystone blocks. The sequence corresponds to the black curve in Fig. 12

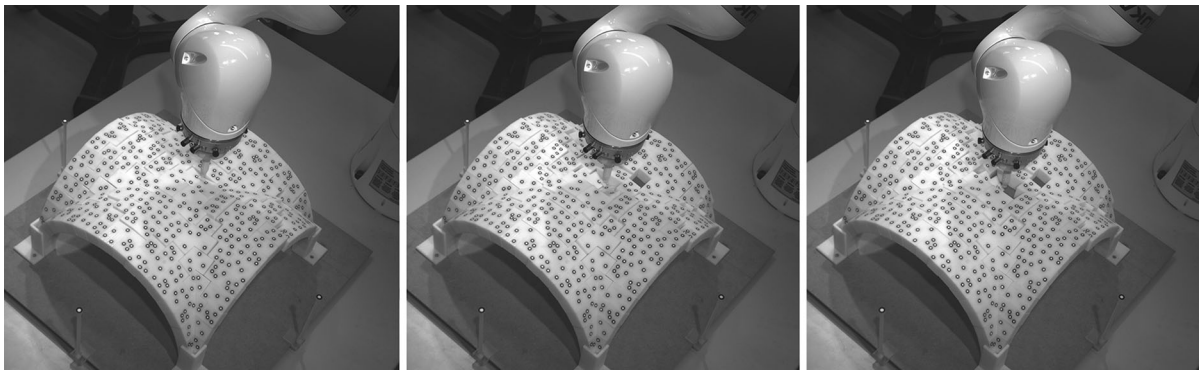

Fig. 14 Point loads: significant stages of load test 2. The point load is applied to only two of the blocks forming the crown. The sequence corresponds to the orange curve in Fig. 12

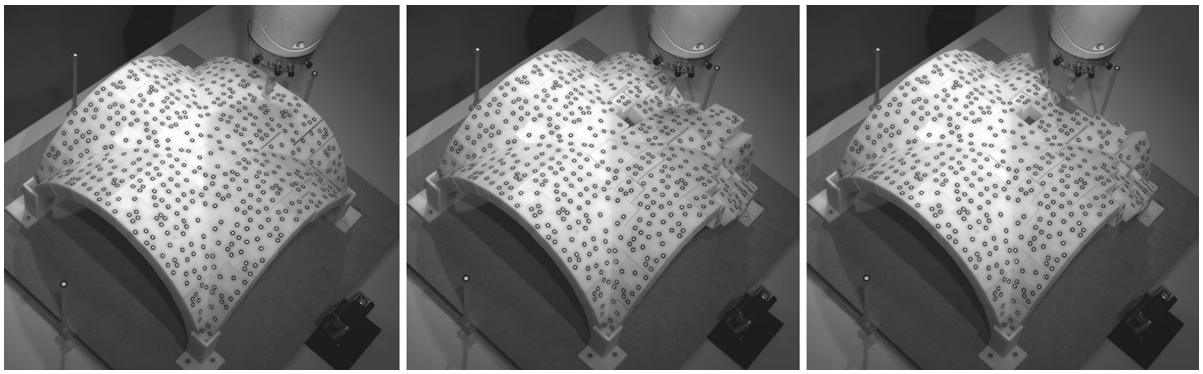

Fig. 15 Point loads: significant stages of load test 5. The point load is applied to a block close to the edge of on one of the webs of the vault. The sequence corresponds to the red curve in Fig. 12

decrease of the resistance of the vault while the slipping block generates less and less friction with the surrounding blocks. In case of the latter, disappearance of the resistance of the vault is sudden.

5.2 Support settlements

In this test case, we move one of the supports of the vault at a constant speed of 1 mm/s in the direction of the horizontal thrust measured at the end effector,

while constraining the movement to the horizontal plane (Fig. 16). Figure 17 shows the position of the end effector as a function of time. The relationship is linear in the X and Y axes. The Z position obviously stays constant at $Z = 0$. The final position of the end effector is $X = 19$ mm, $Y = -11$ mm, and $Z = 0$ mm. This corresponds to displacement vectors with comparable total lengths of approximately 22 mm. The force versus displacement graphs are depicted in Fig. 18. The X and Y components of the force drop from an initially higher value ($F_x = 6$ N, $F_y = 3$ N) to a minimum during the first few seconds of the test, and then gradually increase again until collapse at $F_x = 6$ N and $F_y = 3$ N. The X component is consistently higher than the Y component, which corresponds to the consistently higher and more rapid change in X and Y position of the end effector (Fig. 17). The Z component initially decreases and then remains more or less constant. The observed collapse sequence is depicted in Fig. 19. The collapse caused by the constrained movement is characterised by the formation of a large diagonal crack in the direction perpendicular to the movement of the support. Furthermore, we can observe the formation of typical 2D hinging mechanisms in the boundary arches of the webs adjacent to the moving support. Consistent with the measured behaviour, the mechanism progresses faster in the web with boundary arch parallel to the X axis along which the displacement of the support is the largest. Full collapse of the structure occurs when this web

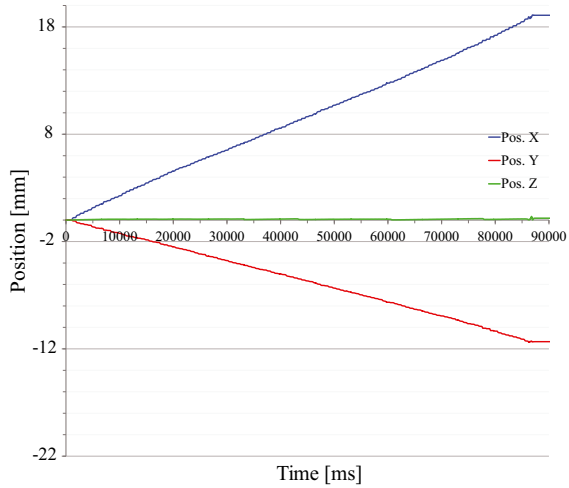

Fig. 17 Support settlements: position of the end effector as a function of time

becomes unstable. Note that this test showed that the vault's geometry is not perfect, resulting in a thrust direction that is not along the diagonal. This is due to the slight differences in the geometry of the voussoirs and slight asymmetry of the scaffolding on which the vault is assembled. As the blocks are always used in the same position and the orientation of the scaffolding is also always the same, this consistently produces slightly asymmetrical results in the measurements.

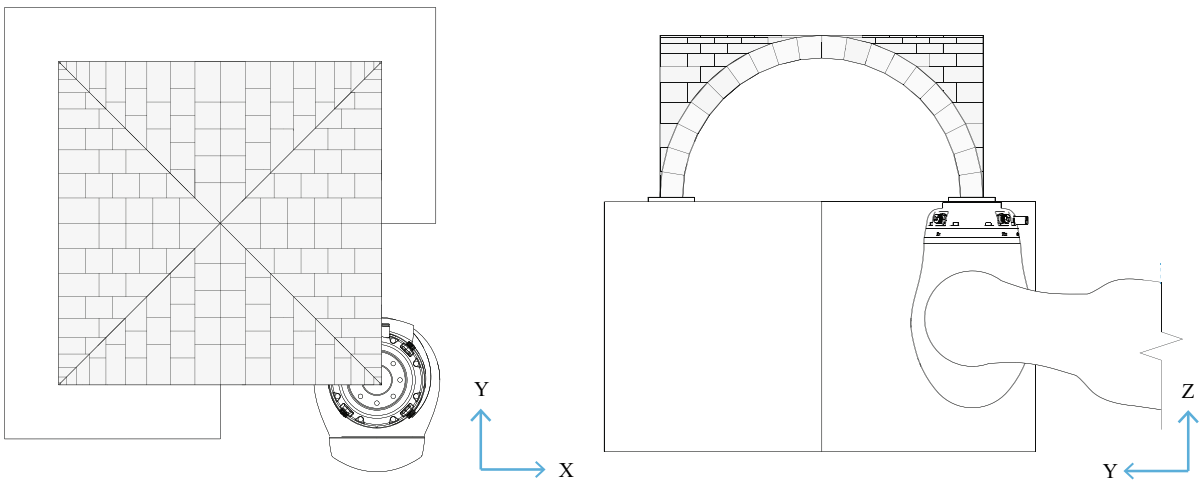

Fig. 16 Support settlements: configuration of the testing setup for the first two support displacement tests in which the displacement of one support is simulated

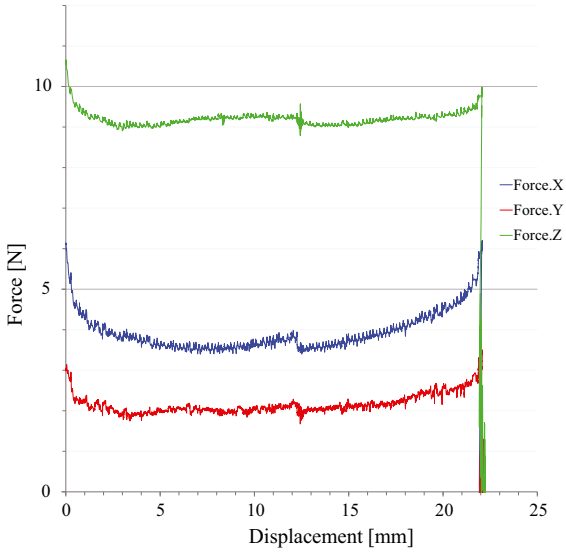

Fig. 18 Support settlements: forces along *XYZ* axes, as a function of the displacement of the end effector

5.3 Soil consolidation

Here, we simulate settlement of the vault into a new configuration caused by differential settlement of the (imaginary) supporting soil, followed by soil consolidation. Two supports of the vault are moved simultaneously but independently by two robotic arms at a constant velocity of 1 mm/s (Fig. 20). Their respective positions are depicted in Fig. 21 as a function of time. Initially, both supports are moved only vertically to simulate settlement of the soil. The first support is moved 5 mm in the Z direction, and the second one 10 mm. Having reached their vertical target positions, the supports are moved further by the robotic arms in the direction of the components in the YZ plane of the measured thrust. To simulate consolidation of the soil, the robots are programmed to decrease the displacement increments exponentially as the settlement progresses. After approximately 277 s, the displacement reduces to zero, and the vault reaches a new, deformed equilibrium configuration. The force/displacement graph of the two supports is depicted in Fig. 22. At 5 mm of vertical displacement, the Y component of the measured thrust at the end effectors of the robotic arms is 5 N in both cases. The measured Z component at that stage is 10 N for both arms. Thereafter, the thrust components in the Y and Z direction at the first support immediately decrease, while the Y and Z components at the second support increase. Then, after the second support reaches its vertical target position at $Z = -10$ mm (and then continues to move in the direction of the measured thrust in the YZ plane, like the first support), the Y and Z components at both supports slowly increase until the final configuration is reached (Fig. 23).

6 Discussion

In this paper, we presented a novel approach to the physical modelling of the collapse behaviour of masonry vaults using 3D-printed scale models, an optical measuring system, and force-sensitive robotic arms. The main advantages of this method are summarised in the following. With force-sensitive robotic arms, different types of tests can be performed on the same model, simply by changing the function and pose of the robots in the tests, rather than

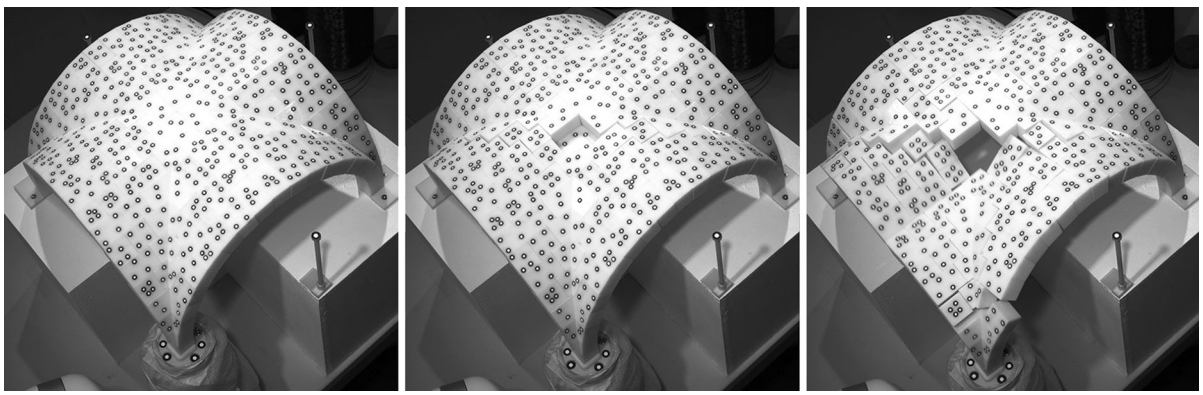

Fig. 19 Support settlements: significant stages of the collapse sequence

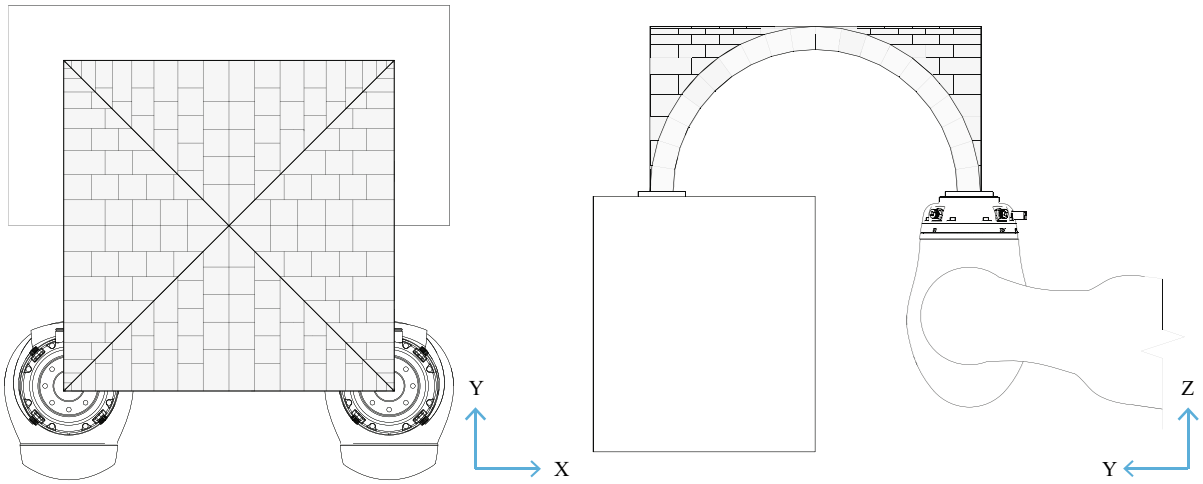

Fig. 20 Configuration of the testing setup for the support displacement tests in which the displacement of two supports of the vault is simulated

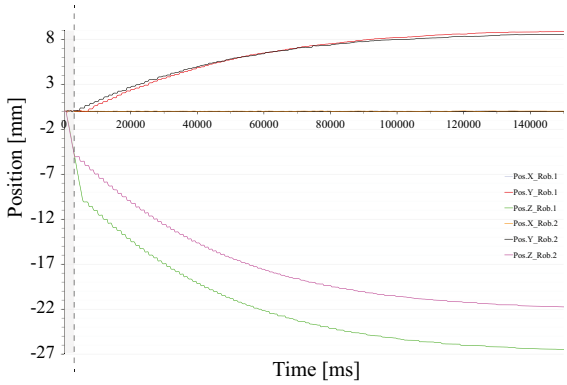

Fig. 21 Soil consolidation: position of the end effector as a function of time

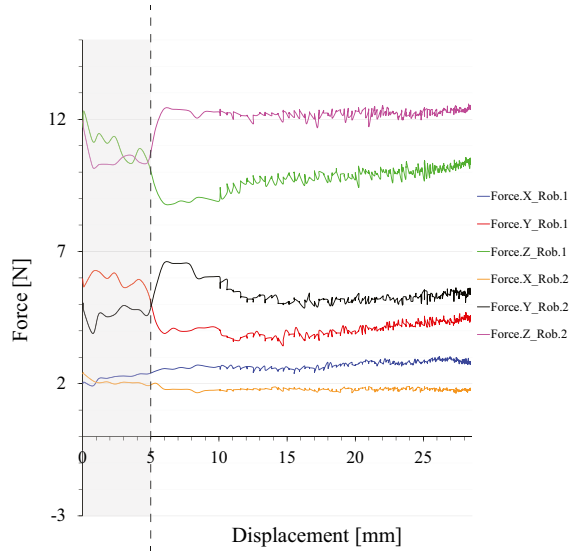

Fig. 22 Soil consolidation: force components along the *XYZ* axes, as a function of the displacement of the end effectors

modifying or rebuilding the entire testing setup. For example, since the robots can be programmed to apply any force to the scale model with a controlled position, direction, sense, and magnitude, the effect of different point-load cases on the development of collapse mechanisms can be investigated easily and flexibly while simultaneously measuring the resistance of the vault to the applied loads. In addition, using real-time feedback about the forces acting on the end effectors of the robotic arms, differential support settlement experiments can be performed in which the trajectory of the displacements is not predetermined, but rather a function of the otherwise unknown outward thrust of the vault. Finally, since the geometry and structural response of the vault can be accurately measured, experiments with the proposed setup can provide valuable benchmarking and calibration data for parametric studies of the influence of vault geometry and boundary conditions on the development of collapse mechanisms using computational simulations based on, for example, Discrete Element Modelling. The main limitation of this method is that the size and weight of the model are constrained by the maximum payload of the robotic arms and the range of the in-house measuring system. Because of this, the forces acting on the end effectors are reduced to a range of

Fig. 23 Soil consolidation: sequence of images captured during the simulation

0–30 N. At this range, the ratio between the noise, caused by the vibration of the robotic arm, and the obtained values is proportionally large.

Acknowledgements This research is supported by the NCCR Digital Fabrication, funded by the Swiss National Science Foundation (NCCR Digital Fabrication Agreement # 51NF40-141853).

Compliance with ethical standards

Conflict of interest The authors declare that they have no conflict of interest.

References

1. Addis B (2005) A history of using scale models to inform the design of structures. Instituto Juan de Herrera, Madrid, pp 9–14
2. Albu-Schäffer A, Haddadin S, Ott Ch, Stemmer A, Wimböck T, Hirzinger G (2007) The DLR lightweight robot: design and control concepts for robots in human environments. Ind Robot Int J 34(5):376–385. doi:10.1108/01439910710774386
3. Andrews Larry (2001) A template for the nearest neighbor problem. C/C++ Users J 19(11):40–49 ISSN 1075-2838
4. Besl Paul J, McKay Neil D (1992) A method for registration of 3-d shapes. IEEE Trans Pattern Anal Mach Intell 14(2):239–256. doi:10.1109/34.121791 ISSN 0162-8828
5. Bischoff R, Kurth J, Schreiber G, Koeppe R, Albu-Schäffer A, Beyer A, Haddadin S, Stemer A, Grunwald G, Hirzinger G (2010) The lightweight robot arm a new reference platform for robotics research and manufacturing. In: ISR/robotik, pp 741–748
6. Danyzy A (1732) Méthode générale pour déterminer la résistance qu'il faut opposer à la poussée des voûtes. Histoire de la Société des Sciences établie à Montpellier 2:40–56
7. Garcia S (1991) Compendio de architectura y simetría de los templos. Colección "Tratadistas Castellano-Leoneses", 1991. Colegio Oficial de Arquitectos en Valladolid, 1681
8. GOM. Optical Measuring Techniques. http://www.gom.com/, 2016. Accessed Oct 21 2016
9. Heyman J (1995) The stone skeleton: structural engineering of masonry architecture. Cambridge University Press, Cambridge
10. Huerta S (2006) Geometry and equilibrium: the gothic theory of structural design. Struct Eng 84(2):23–28 ISSN 1466-5123
11. KUKA. KUKA Industrial Robots. http://www.kuka-robotics.com/, 2016. Accessed Oct 21 2016
12. Ochsendorf J (2006) The masonry arch on spreading supports. Struct Eng 84(2):29–35
13. Quiñonez A, Zessin J, Nutzel A, Ochsendorf J (2010) Small-sale models for testing masonry structures. Adv Mater Res 133–134:497–502. doi:10.4028/www.scientific.net/AMR.133-134.497
14. Rhinoceros. NURBS modelling for Windows. http://www.rhino3d.com/, 2016. Accessed Oct 21 2016
15. Rossi M, Calderini C, Lagomarsino S (2016) Experimental testing of the seismic in-plane displacement capacity of masonry cross vaults through a scale model. Bull Earthq Eng 13(10):261–281. doi:10.1007/s10518-015-9815-1
16. Rossi M, Barentin CC, Van Mele T, Block P (2017) Experimental study on the behaviour of masonry pavilion vaults on spreading supports. Structures 11:110–120. doi:10.1016/j.istruc.2017.04.008 ISSN 2352-0124
17. Stratasys. 3D Printing Solutions. http://www.stratasys.com/, 2016. Accessed Oct 21 2016
18. Theodossopoulos D, Sinha BP, Usmani AS, Macdonald AJ (2002) Assessment of the structural response of masonry cross vaults. Strain 38(3):119–127. doi:10.1046/j.0039-2103.2002.00021.x (ISSN 1475-1305)
19. Van Mele T, McInerney J, DeJong M, Block P (2012) Physical and computational discrete modelling of masonry vault collapse. In: Jasieńko J (eds) Structural analysis of historical constructions, pp 2552–2560